Rocking-Chair Proton battery Based on a low-cost "Water in Salt" Electrolyte

Beibei Yang[1], Tian Qin[1], Yanyan Du, Yulin Zhang, Jin Wang, Tingting Chen, Ming Ge, Duan Bin Cunwang Ge*, Hongbin Lu **

School of Chemistry and Chemical Engineering, Nantong University, Nantong, Jiangsu, 226019, P.R. China.

E-mail: dbin17@fudan.edu.cn; gecunwang@ntu.edu.cn; luhb@nju.edu.cn

Experimental Section

Synthesis of nanobelt structural MoO_3: In typical procedure (**Figure S1**), 1.0 g $(NH_4)_6Mo_7O_{24}\cdot 4H_2O$ was dissolved in 30 mL deionized water and 3 M HNO_3 solution (10 mL) was added to adjust pH. After stirring for 20 min, the mixed solution was transferred into a Teflon-lined stainless steel autoclave, which heated at 180℃ for 24 h. The white precipitate was obtained by centrifugation and washed for several times with deionized water and ethanol. Finally, the obtained product was dried at 60 ℃ overnight.

Synthesis of nickel ferrocyanide (Ni-PBA): Ni-PBA was synthesized by a typical chemical precipitation method (**Figure S2**). To substitute the Fe species in $K_4Fe(CN)_6$ for Ni, 3 mmol of $K_4Fe(CN)_6\cdot 3H_2O$ and 12 g of KCl was dissolved in DI water to 150 mL under stirring to produce a yellow solution A. In addition, solution A was obtained by adding 6 mmol of $NiCl_2\cdot 6H_2O$ to another 150 mL of DI water, following by a vigorous stirring for 30 min. Then, solution A was dropwise added into solution B with magnetic stirring under 75 ℃ for 4 hours. After cooling to room temperature, the precipitate was centrifuged and washed with DI water and ethanol three times per agent. Finally, the as-prepared light green product was vacuum -dried under 60 ℃ overnight.

Physical Characterization: Scanning electron microscopy (SEM) images were collected by a HitachiS-3400 SEM instrument, transmission electron microscopy (TEM) images were obtained on a ThermoFisher Scientific Talos F200x G2 STEM equipment. X-ray diffraction (XRD) of the as-prepared samples were characterized by a Bruker D8 endeavor X-ray diffractometer, equipped with Cu Kα (λ = 0.15405 nm) radiation (40 kV, 40 mA). Thermogravimetric analysis (TGA) was carried out on PerkinElmer TGA 7 analyzer at a heating rate of 10 °C min^{-1}. The measured temperature was raised from 25 to 800 °C under constant air flow (40 mL min^{-1}), and nitrogen was used as a protective gas. X-ray photoelectron spectroscopy (XPS) was carried out via a XSAM800 Ultra spectrometer.

Electrochemical Characterization: To prepare an electrode film, the MoO_3 anode was fabricated by mixing with active materials (70%), Ketjen black (KB, >99.9%, Sinopharm) and polytetrafluorethylene binder (PTFE, 20 wt. % dispersion in H_2O) produce a homogeneous slurry and then form a suitable film by the roll press machine. The preparation of Ni-PBA film was almost the same except that the mass ratio was 6:3:1 due to its relatively poor electro-conductivity. The obtained slurry was rolled into an active material membrane and dried at 80 °C overnight in air. The electrochemical performance was tested in a three-electrode cell, which composed of active materials as the working electrode, a large amount of activated carbon as the counter electrode (a film prepared according to the mass ratio 8:1:1), saturated calomel electrode (SCE) as the reference electrode (E=0.241 vs. standard hydrogen electrode, SHE). Cyclic voltammetry (CV) was performed using an electrochemistry workstation (CHI 650D) at various rate. Galvanostatic charge/discharge (GCD) measurements were performed by LAND CT2001A battery test system (Wuhan LAND electronics). During the preparation of the full cell, charges stored at both cathode and anode should be balanced. Therefore, theoretically, the weight ratio of Ni-PBA cathode and MoO_3 anode should 1: 1.1. The capacity of full cell is measured based on the mass of total Ni-PBA cathode and MoO_3 anode.

Table S1. Crystallographic data and powder XRD Rietveld refinement results for Ni-PBA.

Crystal System		face-centered-cubic		
Space Gro*up*		F*3(202)		
Lattice Parameter		a= b=c=10.07 (Å) V=1021.2		
		α = β = γ = 90°		
		R_{wp}=2.7%, R_B=2.0%		
Atom	x/a	y/b	z/c	SOF
K1	1.00	0.25	0.25	1.00
K2	1.00	0.75	0.75	1.00
Ni1	1.00	0.50	0.50	1.00
Fe1	1.00	0.00	0.00	1.00
C1	1.00	0.19	0.00	1.00
N1	0.31	0.00	0.00	1.00

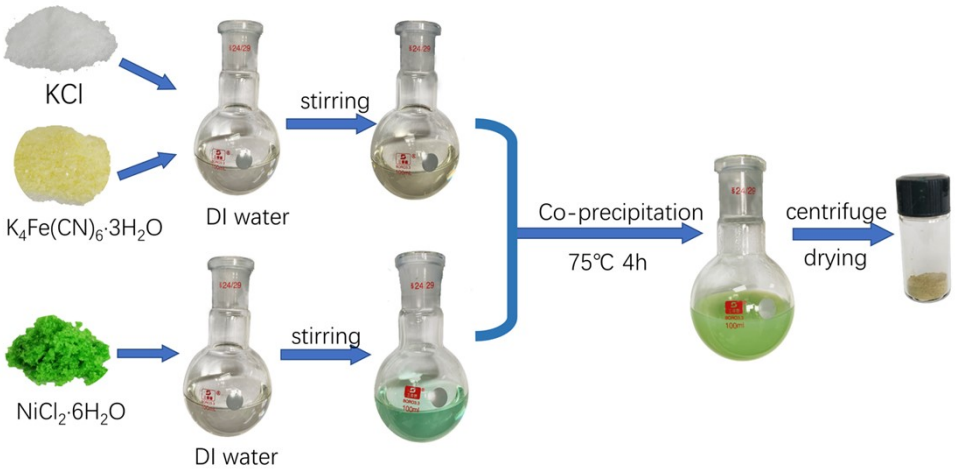

Figure S1. Schematic illustration of synthetic procedure of Ni-PBA.

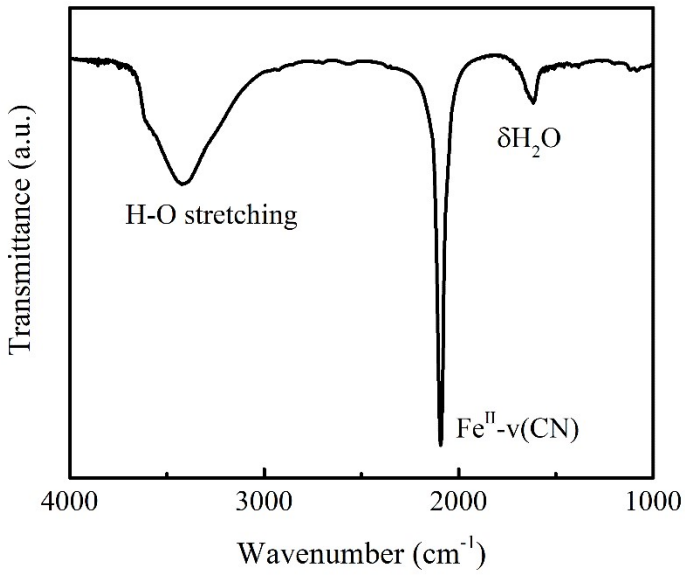

Figure S2. Fourier transform infrared spectroscopy (FT-IR) of Ni-PBA samples. (a strong peak at 2090 cm^{-1} can be classified as the stretching vibration of the triple bond of cyanide-coordinated Fe^{2+}, H-O stretching can be produced from the interstitial water in Ni-PBA)

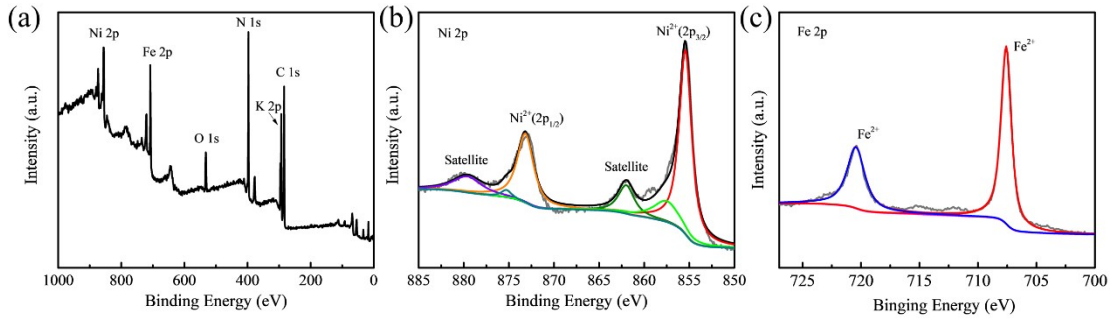

Figure S3. (a) XPS spectra of full survey, (b) high-resolution XPS spectra of Ni 2p and (b) Fe 2p in the as-prepared Ni-PBA. (The Ni 2p spectrum manifest the two main peaks at 873.9 and 855.5 eV correspond to Ni (II) valence of Ni $2p_{1/2}$ and Ni $2p_{3/2}$, respectively. Two characteristic peaks at 720.4 and 707.6 eV were assigned to Fe (II) valence of Fe $2p_{1/2}$ and Fe $2p_{3/2}$.)

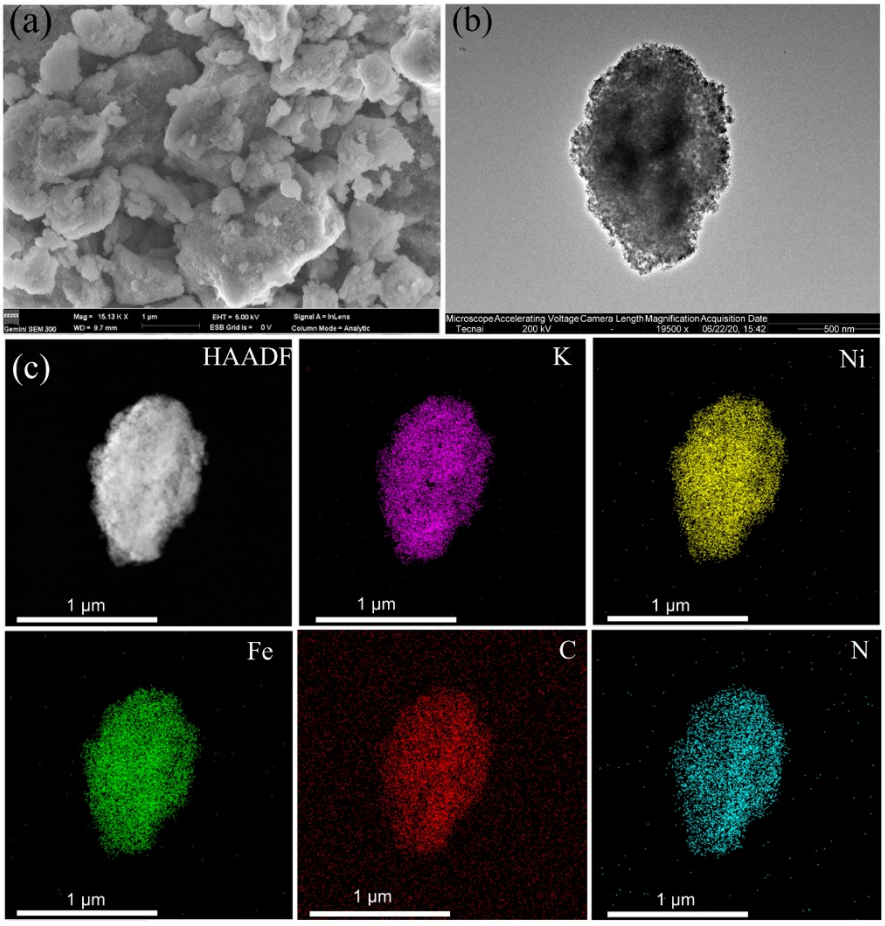

Figure S4. (a) SEM, (b) low amplification TEM, (c) HAADF-STEM image and EDS mapping of Ni-PBA sample.

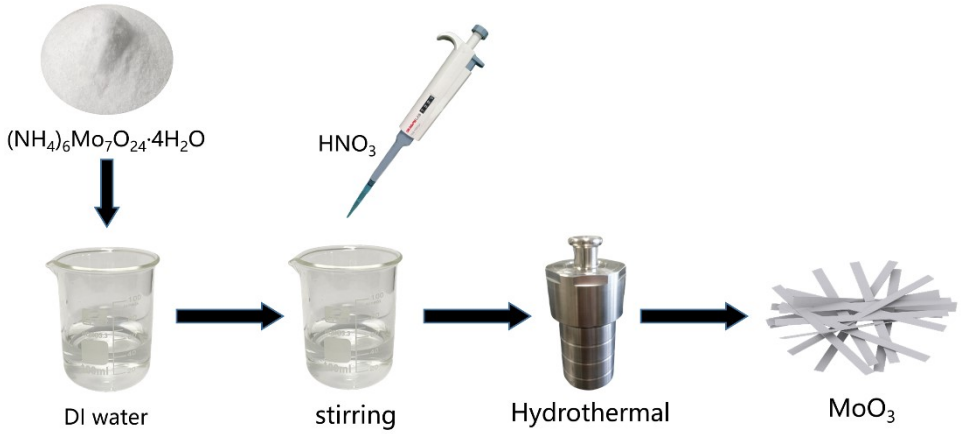

Figure S5. Schematic illustration of synthetic procedure of MoO_3.

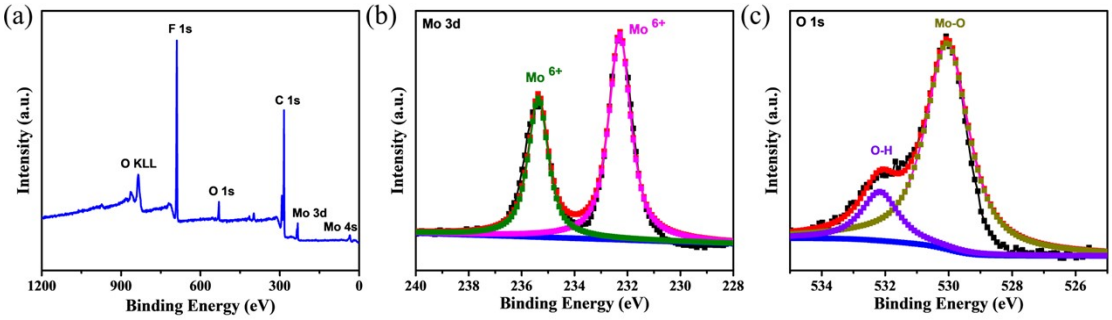

Figure S6. (a) XPS spectra of full survey, (b) high-resolution XPS spectra of Mo 3d and (b) O 1s in the as-prepared MoO_3. (The Mo 3d spectrum manifest the two main peaks at 235.4 and 232.3 eV correspond to Mo (VI) valence of Mo $3d_{5/2}$ and Mo $3d_{3/2}$, respectively.)

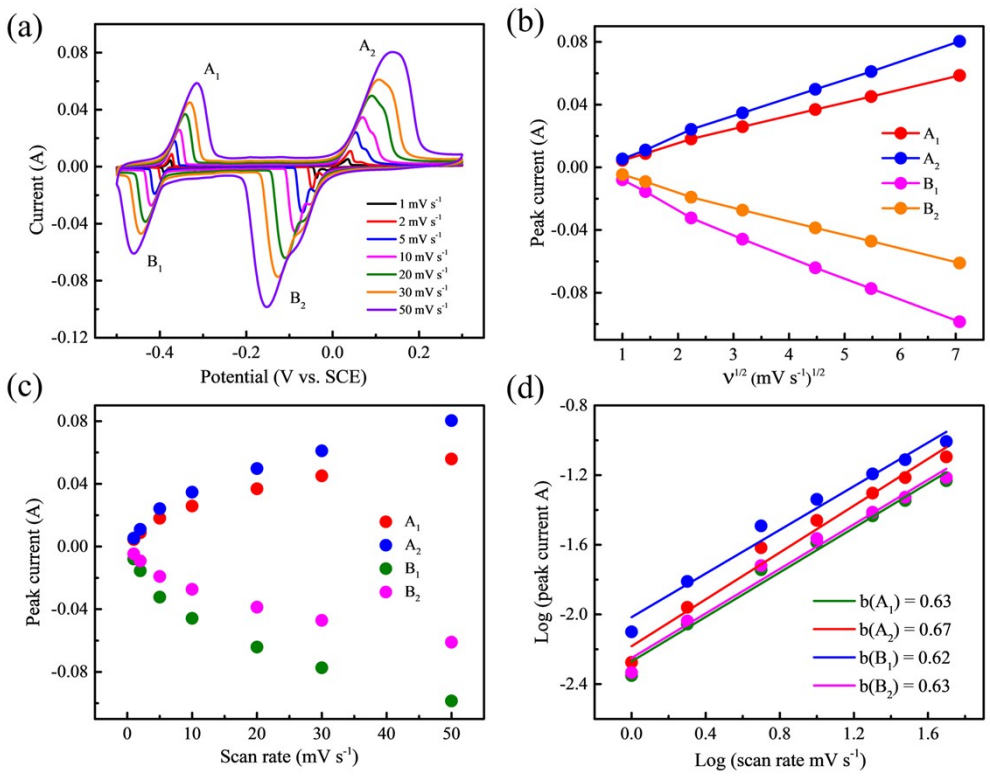

Figure S7. Electrochemical behavior of MoO_3 anode in 1 M H_2SO_4 solution. (a) CV curves (b) The plots of peak currents with respect to square root of scan rates. (c) Plots of the peak currents and scan rates. (f) b values calculated from the lines by plotting log(i) as a function of log(υ). (The electrode shows two cathodic peaks at -0.31 and -0.14 V that is associated with the reduction of Mo^{6+} to Mo^{4+} corresponding to the insertion of hydrogen ions, whereas the anodic peaks around at -0.46 and -0.1 V corresponding to the de-intercalation of hydrogen ions)

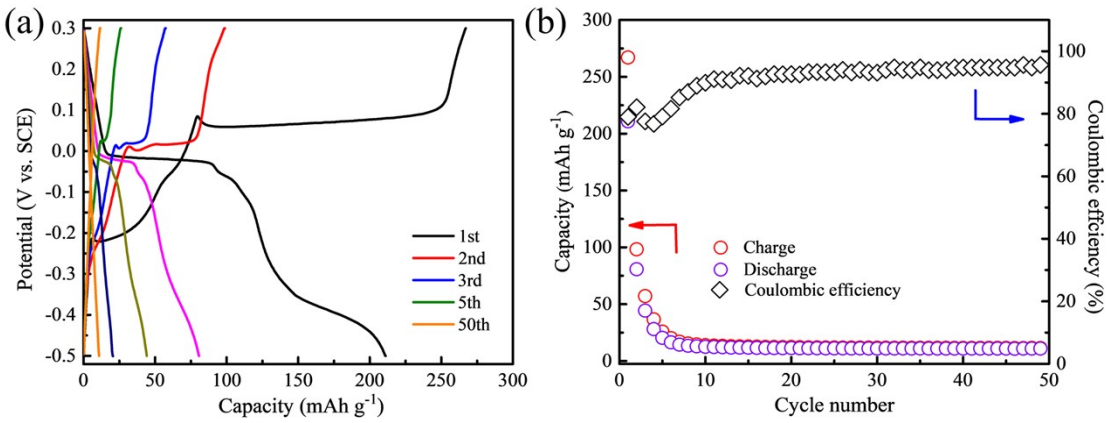

Figure S8. Selected GCD profiles and (c) cycle performance of MoO_3 anode in 1 M H_2SO_4 at a current density of 1 A g^{-1}.

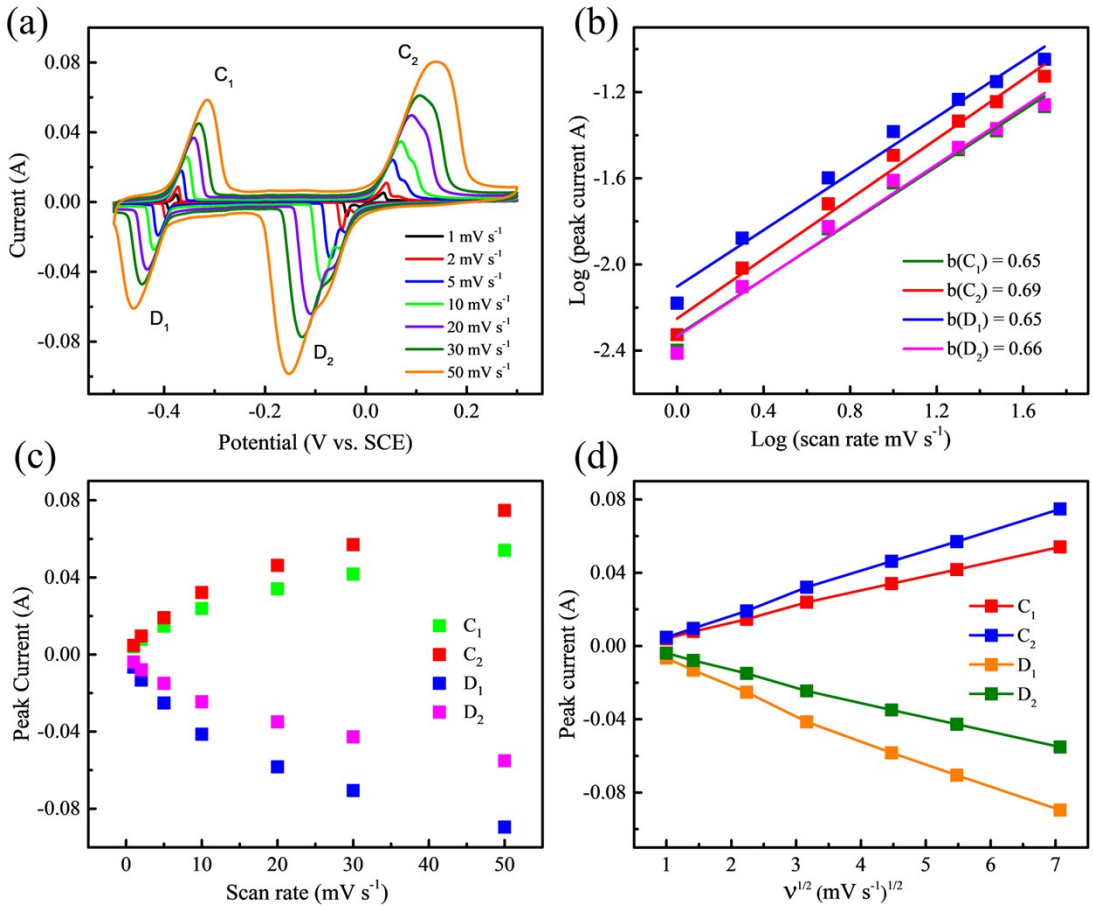

Figure S9. Electrochemical behavior of MoO_3 anode in 2 M HCl solution. (a) CV curves (b) The plots of peak currents with respect to square root of scan rates. (c) Plots of the peak currents and scan rates. (f) b values calculated from the lines by plotting log(i) as a function of log(υ).

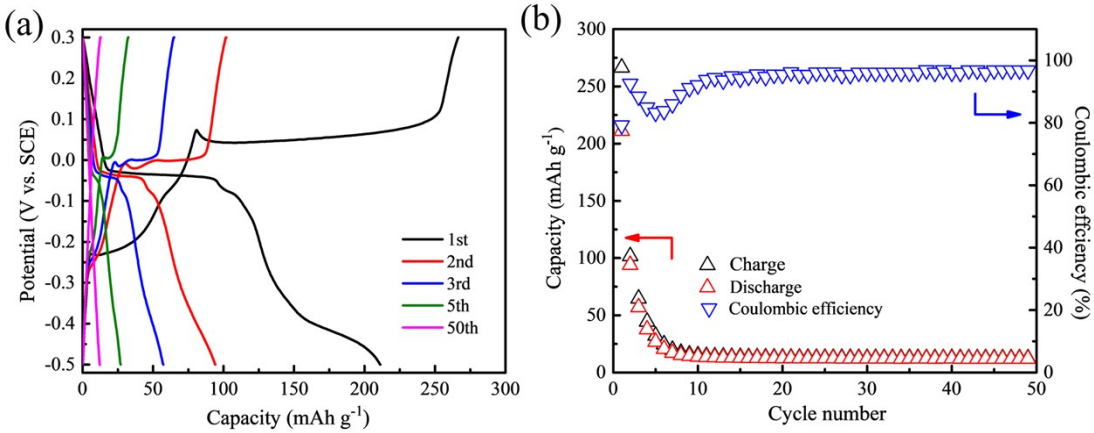

Figure S10. Selected GCD profiles and (c) cycle performance of MoO_3 anode in 2 M HCl solution at a current density of 1 A g^{-1}.

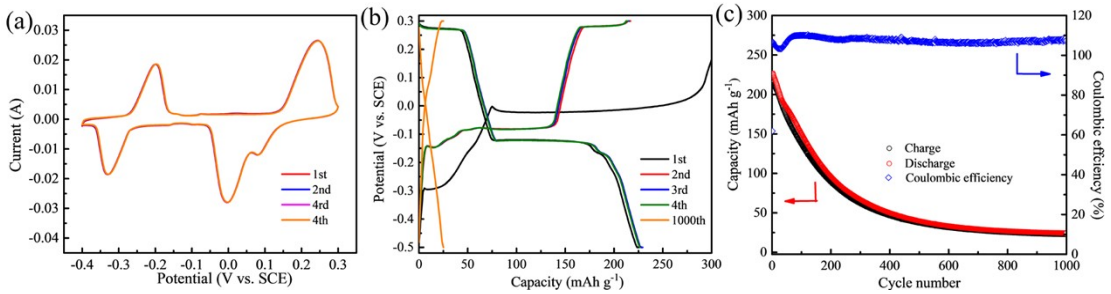

Figure S11. Electrochemical performance of MoO_3 anode in 1 M HCl+5 M $ZnCl_2$ solution. (a) CV curves at 1 mv S^{-1}, (b) the corresponding GCD curves at different cycles and (c) cycling performance at 1 A g^{-1}.

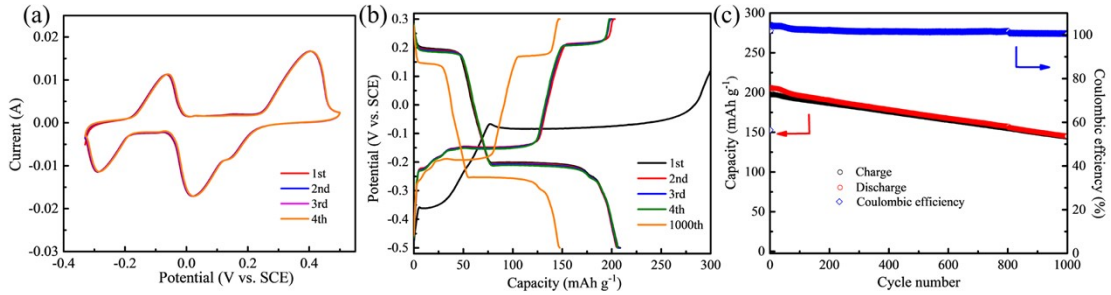

Figure S12. Electrochemical performance of MoO_3 anode in 1 M HCl+10 M $ZnCl_2$ solution. (a) CV curves at 1 mv S^{-1}, (b) the corresponding GCD curves at different cycles and (c) cycling performance at 1 A g^{-1}.

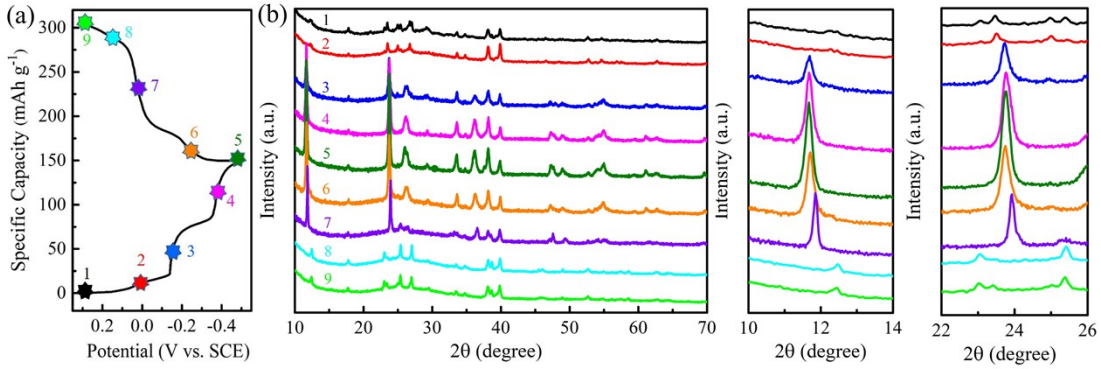

Figure. S13. (a) A typical discharge-charge curve and (b) Ex situ XRD patterns of the MoO_3 electrode at the selected states of second cycle, as marked from state 1 to 9. (When discharged to -0.5 V, the diffraction peaks for MoO_3 electrode located at 12.3 and 25.3 ° almost disappear, while some new strong peaks appear at 11.8 and 23.8 °, indicating the formation of a newly phase with the proton insertion (State 5). Upon the subsequent charge process, the strong peaks show a positive shift and nearly recover to the pristine state (State 1), further demonstrating the good reversible on the storage process of proton

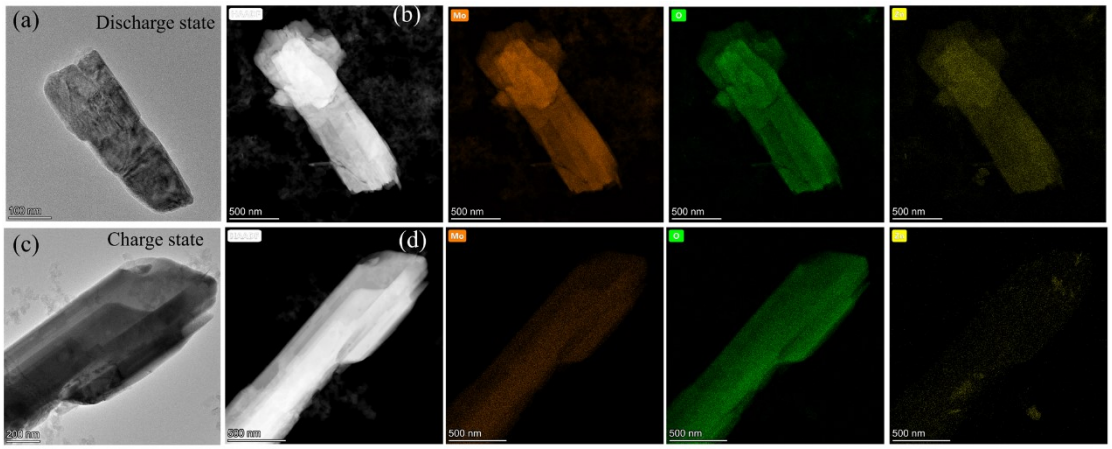

Figure S14. (a, c) TEM images and (b, d) TEM-EDX mappings of MoO_3 anode at the full first discharge (-0.5 V) and charge state (0.3 V).

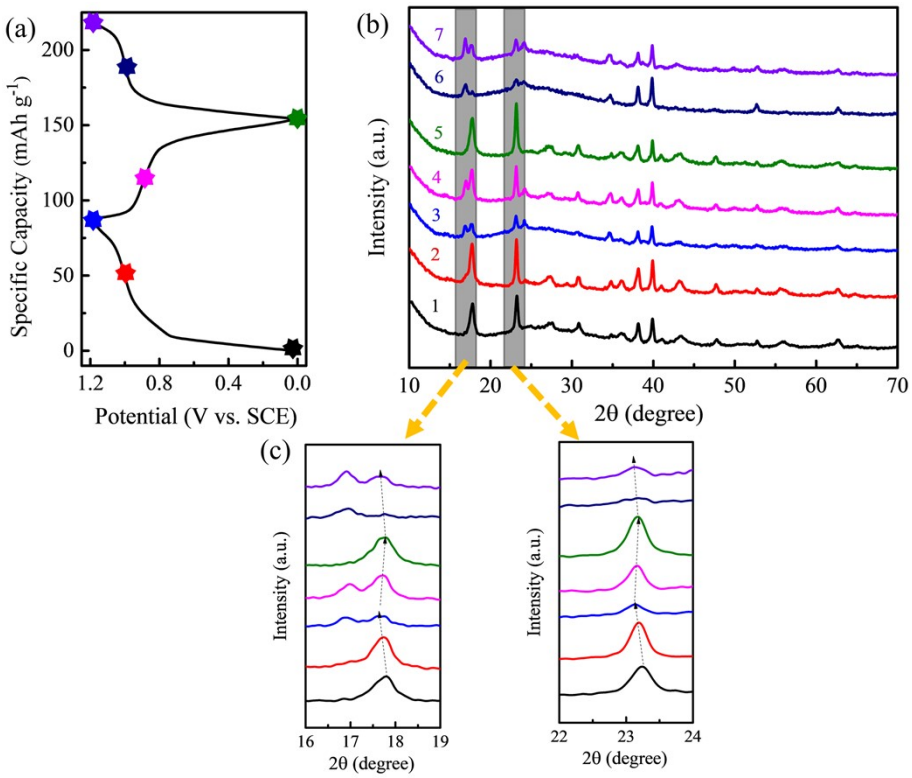

Figure. S15. (a) A typical discharge-charge curve and (b) Ex situ XRD patterns of the Ni-PBA electrode at the selected states of first two cycles, as marked from state 1 to 7. (It displays a clear change during the de-intercalation/insertion process. The peaks at about 17.8 ° and 23.2° shift slightly to the negative position upon first charge, along with the occurrence of a weak peak (17.0°). Upon the following discharge, newly peak is gradually decreased and the above two weak peaks show a slight positive shift owing to the H^+ insertion. Upon the second charge, the XRD pattern reverts back to the first charged state 3, indicating the high reversible of Ni-PBA cathode.)

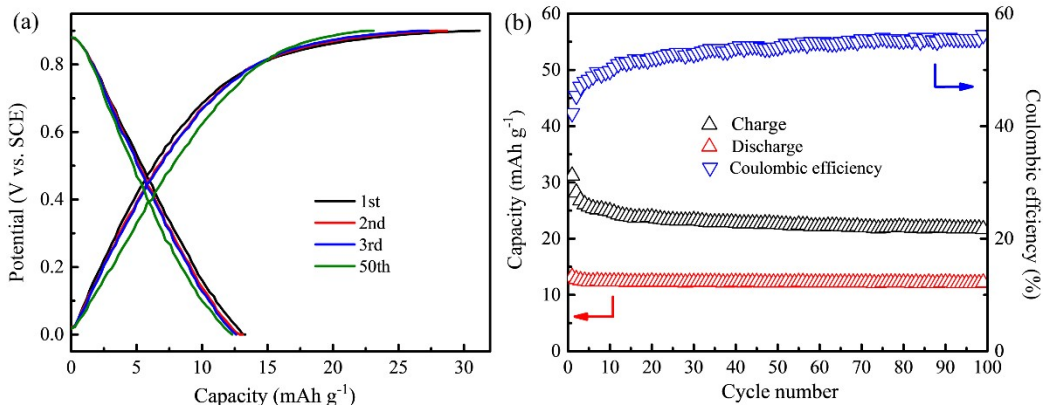

Figure S16. (a) Selected GCD profiles and (c) cycle performance of Ni-PBA anode in 2 $ZnCl_2$ solution at a current density of 0.2 A g^{-1}.

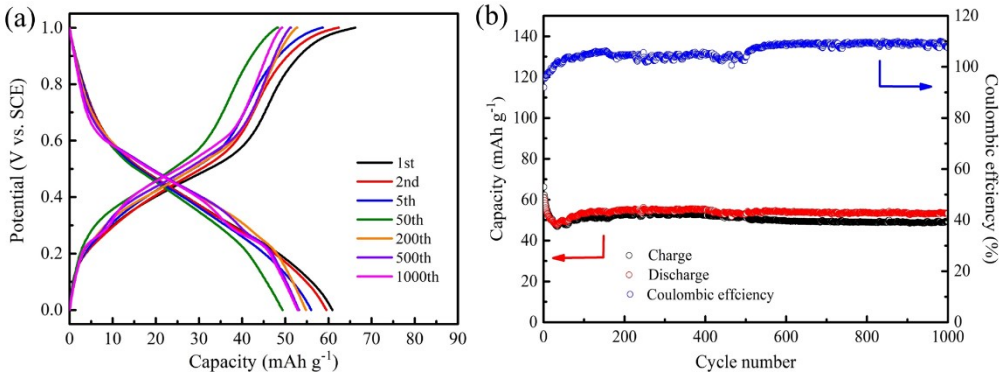

Figure. S17. (a) GCD profiles at different cycles and (b) cycling performance of Ni-PBA electrode in 0.5 M HCl solution at a current density of 0.1 A g^{-1}.